Journal of Biomechanics 44 (2011) 1666–1672

Contents lists available at ScienceDirect

Journal of Biomechanics

journal homepage: www.elsevier.com/locate/jbiomech
www.JBiomech.com

# Patient-specific finite element analysis of the human femur—A double-blinded biomechanical validation

Nir Trabelsi [a], Zohar Yosibash [a,*], Christof Wutte [b,c], Peter Augat [b,c], Sebastian Eberle [b,c]

[a] Department of Mechanical Engineering, Ben-Gurion University of the Negev, Beer-Sheva, Israel
[b] Institute of Biomechanics, Trauma Center Murnau, Murnau, Germany
[c] Institute of Biomechanics, Paracelsus Medical University, Salzburg, Austria

ARTICLE INFO

*Article history:*
Accepted 22 March 2011

*Keywords:*
Femur
Finite element method
Validation
Bone experiments

ABSTRACT

Patient-specific finite element (PSFE) models based on quantitative computer tomography (qCT) are generally used to "predict" the biomechanical response of human bones with the future goal to be applied in clinical decision-making. However, clinical applications require a well validated tool that is free of numerical errors and furthermore match closely experimental findings. In previous studies, not all measurable data (strains and displacements) were considered for validation. Furthermore, the same research group performed both the experiments and PSFE analyses; thus, the validation may have been biased. The aim of the present study was therefore to validate PSFE models with biomechanical experiments, and to address the above-mentioned issues of measurable data and validation bias. A PSFE model (p-method) of each cadaver femur ($n=12$) was generated based on qCT scans of the specimens. The models were validated by biomechanical in-vitro experiments, which determined strains and local displacements on the bone surface and the axial stiffness of the specimens. The validation was performed in a double-blinded manner by two different research institutes to avoid any bias. Inspecting all measurements (155 values), the numerical results correlated well with the experimental results ($R^2=0.93$, slope 1.0093, mean of absolute deviations 22%). In conclusion, a method to generate PSFE models from qCT scans was used in this study on a sample size not yet considered in the past, and compared to experiments in a douple-blinded manner. The results demonstrate that the presented method is in an advanced stage, and can be used in clinical computer-aided decision-making.



## 1. Introduction

Patient-specific finite element (PSFE) modeling based on quantitative computer tomography (qCT) is used to "predict" the biomechanical response of human bones. The computed data (usually displacements, strains and stresses) is interpreted, for example, to "predict" bone fracture risk, optimize implants and diagnose the severity of osteoporosis. These PSFE models are advocated for use in clinical practice (Keaveny, 2010).

Only a limited number of studies were dedicated to the systematic validation of PSFE models of femoral bones by comparison to in-vitro experiments, and not all possible *measurable data* (strains and displacements) were considered. In most studies conventional h-version FE methods (h-FEMs) were used (see e.g. (Keyak et al., 1990; Cody et al., 1999; Helgason et al., 2008b; Schileo et al., 2007)) having mostly inhomogeneous distribution of isotropic material properties obtained by assigning constant distinct values to different elements, causing the material properties to become mesh dependent (Taddei et al., 2007). Furthermore, usually only strains were reported and usually on a small cohort of bones. For example, in Helgason et al. (2008b) a single femur was investigated, which did not show a satisfactory correlation between computed and measured strains (stresses were though well correlated). Good predictions for strains are reported by Schileo et al. (2007) and latter improved in Schileo et al. (2008) on a larger cohort (8 femurs, showing a correspondence between PSFE and experiments of $R^2=0.91$, 0.95 and slope 1.01, 0.97) and by Bessho et al. (2007) on a cohort of 11 femurs.

Recent studies on qCT based patient-specific high-order FEs (PSHOFE) with inhomogeneous material properties were shown to predict very well both strains and displacements on a cohort of three femurs and various loading scenarios (Yosibash et al., 2007a; Trabelsi et al., 2009). In all previous studies both the experiments and PSFE/PSHOFE analyses were performed by the same group, thus the validation may have been biased. However, clinical applications require a well validated tool, i.e. it is required to demonstrate (first in-vitro) that the PSFE results are free of numerical errors and furthermore match closely experimental findings—a requirement which to our opinion has not yet been fully met.

* Corresponding author.
*E-mail address:* zohary@bgu.ac.il (Z. Yosibash).

0021-9290/$ - see front matter © 2011 Elsevier Ltd. All rights reserved.
doi:10.1016/j.jbiomech.2011.03.024

The aim of the present study was therefore to validate PSHOFE models with biomechanical experiments, by comparing all measurable quantities—strains, displacement magnitudes and overall bone stiffness. Furthermore, the validation was accomplished with a sufficiently large sample of fresh-frozen bone specimens ($n=12$) by two different research institutes in a double-blinded process to avoid any bias.

## 2. Materials and methods

A PSHOFE model of each human cadaver femur was generated based on qCT scans of the specimens. The reliability of these models was validated by in-vitro biomechanical experiments, which determined strains and local displacements on the bone surface and the axial stiffness of the specimens. The validation was performed in a double-blinded manner by two different research institutes. The first institute (BGU) generated the PSHOFE models and performed the FEAs, and was blinded to the experimental results. The FEAs were based on qCT-scans, information about the experimental setup, and measurement locations, provided by the second institute (TCM). The second institute performed the biomechanical experiments and was blinded to the FEAs. The final comparison of FEAs and experimental results was performed by the second institute.

### 2.1. In-vitro experiments

Biomechanical tests on human cadaver femurs were conducted to determine strains and local displacements on the bone surface and the axial bone stiffness. Twelve human femurs (six pairs, age $56\pm5.6$yrs, range 48–64, 2 female and 4 male donors) were tested. Table 1 summarizes the femurs' data (from each donor both right and left femurs are used).

Prior to testing, qCT-scans (Lightspeed VCT, GE Healthcare, Waukesha, WI; USA) were conducted including a mineral density calibration phantom (HEAD CT Calibration Phantom, Mindways, Austin, TX, USA) to determine the relation between Houndsfield units (HU) and bone mineral density (BMD).

The fresh-frozen femurs were thawed for 12 h at 4 °C prior to preparation. All soft tissue was stripped from the bone. Five uniaxial strain-gauges (SGs) were bonded to the surface of the bones. The SGs (KFG-1-120-C1-11L3M3R, Kyowa Electronic Instruments, Tokyo, Japan) were applied to the superior neck, the inferior neck, the lesser trochanter, the medial shaft and the lateral shaft (Fig. 1).

The axes of the SGs were aligned with the femoral neck axis or the femoral shaft axis to measure compressive or tensile strains during axial compression. The SGs were applied to the bone surface according to a valid protocol by Taddei et al. (2006). The SGs were linked to an amplifier (Spider 8, Hottinger Baldwin Messtechnik, Germany) and a personal computer to record the data by software (Catman easy, Hottinger Baldwin Messtechnik, Germany).

The specimens were then prepared for biomechanical testing in a single leg loading configuration (Eberle et al., 2009). The distal end of each femur was potted with casting resin (RENCAST FC53, Huntsman Advanced Materials, Bergkamen, Germany) in an aluminum case that fitted into a cardan joint. The femoral head was potted in a hemisphere of casting resin that fitted the proximal adapter of the test setup (Fig. 1b). The embeddings were aligned such that the line of force went through the center of the femoral head and the center of the epicondyles (Fig. 1).

To measure local displacements of the bones, optical markers were applied to points to be measured on the bone surface. Eight to nine optical markers per specimen were distributed over the frontal plane of the bones (Figs. 1 and 2). Further optical markers were applied to the proximal adapter of the testing machine and the frontal part of the cardan joint (Fig. 1b). An optical sensor (PONTOS, GOM, Braunschweig, Germany) tracked the markers. Coordinates, displacements and deformations were calculated automatically for all markers using photogrammetric evaluation procedures (PONTOS, GOM, Braunschweig, Germany).

The prepared femurs were mounted into a servo-electric testing machine (Zwick 010, Zwick GmbH & Co. KG, Germany). The testing machine introduced the machine force by a ball-joint-like support to the femoral head (Fig. 1). The distal end was supported by a biaxial cardan joint (Fig. 1b). This "clamping" results in the most physiological surface strains on femurs according to Speirs et al. (2007). Static axial compression tests with elastic deformation of the specimens were performed with a crosshead speed of 10 mm/min. Testing was performed with three cycles from 0 to 250 N, three cycles from 0 to 500 N, three cycles from 0 to 750 N and three cycles from 0 to 1000 N with a holding time of 10 s per test cycle. The loading was controlled via a load cell that was placed between testing machine and proximal adapter (Serie K, GTM Gassmann Testing and Metrology, Germany).

**Table 1**
Data of donors.

| Donor | Age (years) | Height (cm) | Weight (kg) | Sex |
|---|---|---|---|---|
| 1 | 59 | 180 | 96 | Female |
| 2 | 53 | 193 | 98 | Male |
| 3 | 48 | 170 | 55 | Male |
| 4 | 64 | 168 | 136 | Female |
| 5 | 54 | 178 | 161 | Male |
| 6 | 58 | 185 | 86 | Male |

The bone surface strains were recorded for the full load range and for all test cycles. The strain values at the end of the 10 s holding time at each test cycle were used to calculate a mean value of the three test cycles per load step. These mean values were used for the later comparison with the FEA. The total displacements $u_{tot}\equiv\sqrt{u_x^2+u_y^2+u_z^2}$ of the optical markers on the bone surface (see Fig. 2) were recorded at the end of the 10 s holding at every load cycle. A mean value of the three load cycles was calculated for the later comparison with the FEA. The axial bone stiffness was determined by calculating the slope of the linear force—displacement-curve *of the testing machine* from 200 to 1000 N for all three cycles of the last load level. The mean value of these three cycles was used for the later comparison with the FEA.

### 2.2. Subject-specific high-order finite element models

Prior to testing, qCT-scans (Lightspeed VCT, GE Healthcare, Waukesha, WI, USA) were conducted with the following parameters: helical mode, peak voltage 120 kVp, tube current 90 mAs, 1.0 mm slice thickness and a pixel size of 0.547 or 0.488 mm. The specimens were scanned in air. A mineral density calibration phantom (HEAD CT Calibration Phantom, Mindways, Austin, TX, USA) was scanned with each specimen to determine the relation between Houndsfield units (HU) and bone mineral density (BMD).

The geometry of each femur was extracted from the qCT slices and divided into cortical and trabecular regions using special in-house programs (details are provided in (Yosibash et al., 2007a); (Trabelsi et al., 2009)). Exterior, interface and interior boundaries were traced at each slice followed by a smoothing algorithm applied that generates smooth closed splines used for the solid body generation. The solid body was meshed by an auto-mesher with tetrahedral elements using the p-FE StressCheck[1] code. The typical number of elements representing a femur amounted to 5000 elements. The surfaces of the bone were accurately represented in the FE model by using the blending mapping method (Szabo and Babuska, 1991). The entire algorithm is illustrated in Fig. 3.

*Boundary Conditions:* The boundary conditions applied to the FE model are aimed to mimic the experimental setup. The femoral head was loaded by a total force of 1000 N in the $z$ direction according to the global coordinate system. The plane of loading was inclined in an angle of $\sim6^\circ$ (depending on each experiment conditions) with respect to the horizontal plane. The applied load resultant passes through the center of the femoral head and the center of the epicondyles. The head was free to move in the $z$ direction and spring BCs were defined to lock the head's movements in the $x$ and $y$ directions but allowing head rotation (Fig. 4a). The spring BCs were preferred over displacement BCs based on preliminary numerical investigation. Both femoral head rotation and whole bone deformation were as expected in experimental observation, in addition to decreasing in the model numerical error. The distal face, being placed in the cardan joint, was able to rotate about the $Y$ axis (based on experimental observation the rotation about the $X$ axis is negligible).

A line of rotation (located approximately in the center of the distal face section) was defined as a rigid body constraint. A balance condition was applied to avoid moments in the distal face center. We complemented the BCs by applying anti-symmetry constraints to the distal surface (Fig. 4b).

A summary on boundary conditions in the experiments and as applied in the FE models is provided in Table 2.

*Material properties assigned to the PSHOFE models:* Among the many empirical relations between Young's modulus and bone density, with a constant Poisson's ratio, see e.g. (Cody et al., 2000; Keller, 1994; Keyak and Falkinstein, 2003; Morgan et al., 2003) and the review (Helgason et al., 2008a), we use in our simulations the Keyak & Falkinstein relationship (Keyak and Falkinstein, 2003), which was shown to provide the closest results when compared to in-vitro experiments (see Yosibash et al. 2007a,b; Trabelsi et al., 2009). Young's modulus is given by (2)–(4), while the Poisson ratio is kept constant $\nu=0.3$.

$$\rho_{EQM}=10^{-3}(a\times HU-b)\left[\frac{\text{gm}}{\text{cm}^3}\right] \tag{1}$$

$$\rho_{ash}=1.22\rho_{EQM}+0.0523\left[\frac{\text{gm}}{\text{cm}^3}\right] \tag{2}$$

$$E_{Cort}=10200\,\rho_{ash}^{2.01}\,[\text{MPa}] \tag{3}$$

$$E_{Trab}=5307\rho_{ash}+469\,[\text{MPa}] \tag{4}$$

here $\rho_{EQM}$ is the equivalent mineral density, $\rho_{ash}$ is the ash density of the bone, $E_{Cort}$, $E_{Trab}$ are Young's moduli in the cortical and trabecular regions, respectively, and the parameters $a$ and $b$ are determined by the phantoms in the qCT-scan.

[1] StressCheck is a trademark of ESRD, Ltd., St Louis, MO, USA.

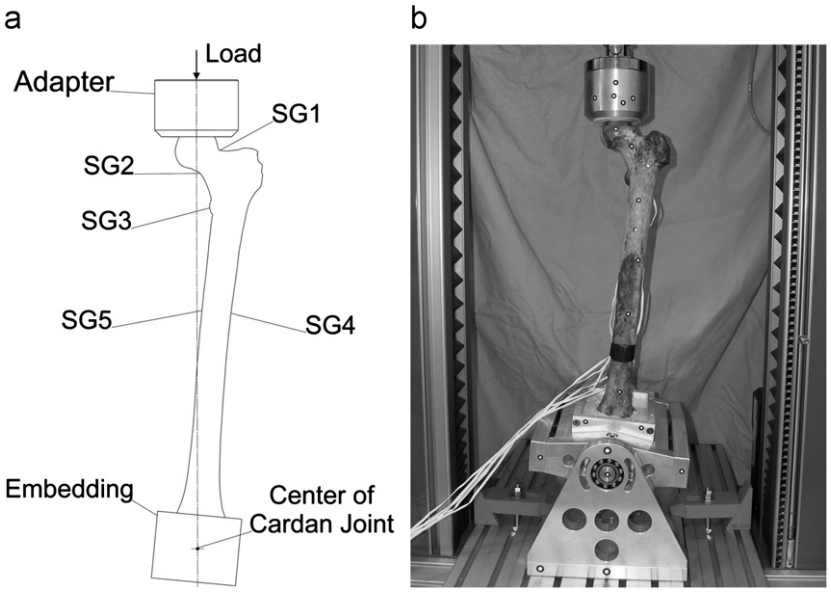


**Fig. 1.** (a-left) Sketch of the frontal plane of an embedded and instrumented left femur. The adapter applied the load by the testing machine to the specimen. The proximal embedding (hidden in adapter) builds a ball-joint with the adapter. Strain gauges (SG1-SG5) are applied to specific anatomic sites. SG1—located at the middle of the superior neck. SG2—located opposite to SG1 at the inferior neck. SG3—ocated next to the most prominent part of the lesser trochanter. SG4—located 100 mm distally to SG3 at the medial side of the shaft. SG5—located opposite to SG4 at the lateral side of the shaft. (b-right) Experimental setup with an embedded an instrumented left femur. Optical markers were distributed over the specimen, the adapter of the testing machine, and the cardan joint.

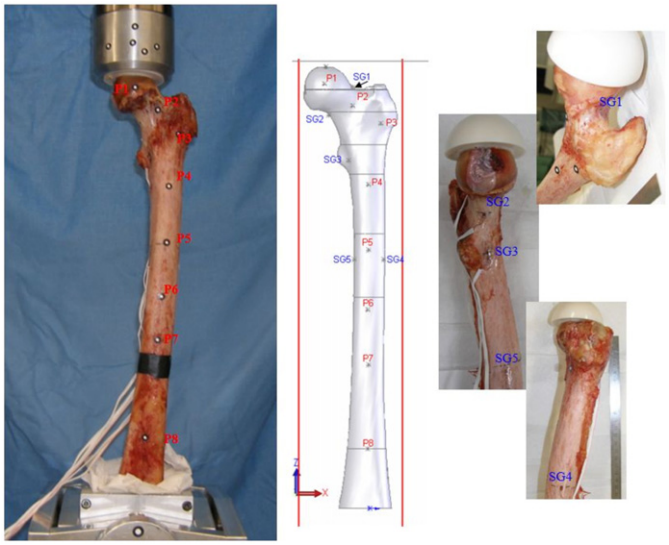


**Fig. 2.** SG locations and location of the points of interest at which displacements are measured.

The solid models were matched to the positions of the optical markers by a best-fit algorithm included in the optical measurement software (PONTOS, GOM, Braunschweig, Germany). Therefore, the positions of the optical markers on the bone surface could be determined. Furthermore, the position of the bones relative to the distal adapter of the testing machine and the cardan joint could be determined. Therefore, the line of force and the cardan center were known and the boundary conditions could be applied properly to the FE model. The positions of the SGs were determined by photographs of the prepared specimens (see Fig. 2).

### 2.3. Validation procedure

Numerical and experimental results were compared and the deviation was calculated for each of the measured parameters. A mean value of the absolute deviations was calculated for every category of measurement (strain, local displacement and stiffness) and for all individual measurements. The corroboration between FEA and experiment was determined by regression analysis for every category (strain, local displacement and stiffness) and for all individual measurements. The quality of the FEA was expressed by the coefficient of linear regression $R^2$, and by the slope and the intercept of the regression curve, following Taddei et al. (2006).

## 3. Results

### 3.1. Experimental results

All tests resulted in repeatable strain values with standard deviations of 0–3% (mean 2%) in-between the three test cycles of each load level. All strain–load-curves showed a linear correlation by at least 98%. All tests resulted in repeatable local displacement values with standard deviations of 2–19% (mean 8%) in-between the three test cycles of each load level. All displacement–load-curves showed a linear correlation by at least 75%. Therefore, the experimental results were analyzed only for the 1000 N load level.

Because of technical problems with the optical measurement system during two tests, the local displacement values of these two specimens had to be discarded. Finally, strain values of twelve specimens (60 measurements), local displacement values of ten specimens (83 measurements) and axial stiffness values of twelve specimens (12 measurements) were used for validation purposes.

### 3.2. Numerical results

The polynomial degree ($p$) over the FE mesh was increased to observe convergence in the numerical results and both errors in energy norm, strains and displacements were monitored to verify the numerical (at $p=6$ or $p=8$ the FE model consists of about 700,000 degrees of freedom (DOF)). An example of the convergence of the numerical results as a function of the number of degrees of freedom is given in Fig. 5 and the magnified deformed configuration in comparison to the experiment is shown for one of the femurs in Fig. 6.

The principal strains were calculated for each SG as the average value on elements' surface, and the principal directions were verified to be aligned with the SG direction in the

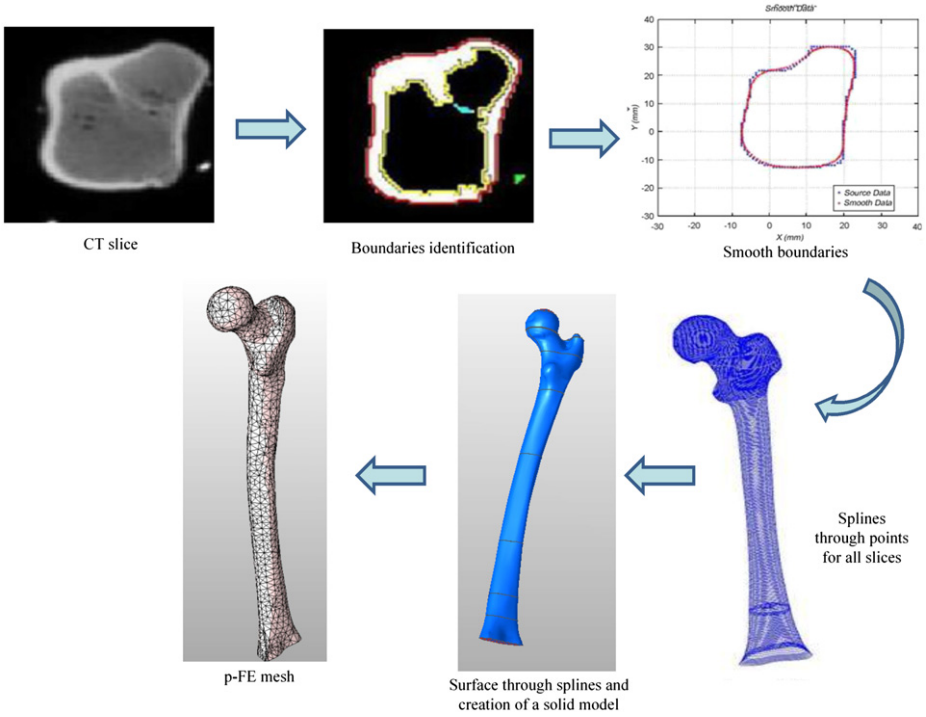


**Fig. 3.** The flowchart for generating the PSHOFE model. From a typical CT-slice → contour identification → smoothing boundary points → close splines for all slices → bone surface and solid model → p-FE mesh.

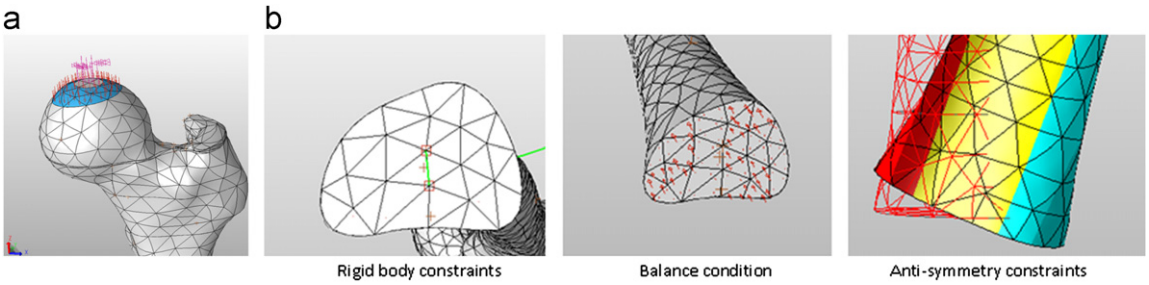


**Fig. 4.** Load on the femur's FE head and constrains at the distal part of FE model.

**Table 2**
Summary on boundary conditions in the experiments and as applied in the FE models.

| | *Femoral head* | | *Distal face* | |
|---|---|---|---|---|
| | *Experiment* | *FE* | *Experiment* | *FE* |
| *X*-translation | Locked by ball joint | Locked by spring | Locked | Locked |
| *Y*-translation | Locked by ball joint | Locked by spring | Locked | Locked |
| *Z*-translation | Free | Free | Locked | Locked at the section center only, & calibrated force applied |
| *X*-rotation | Free | Free | Free (negligible) | Locked |
| *Y*-rotation | Free | Free | Free | Free |
| *Z*-rotation | Free | Locked | Locked | Locked |

experiments. The averaged strain around the SG was shown to be a better measure that needs to be compared to the experiment result (the SG measures an average value over the gauge length). The total displacements $u_{tot} \equiv \sqrt{u_x^2+u_y^2+u_z^2}$ were pointwise computed at each of the measurement points. Bone's stiffness was computed as the ratio of 1000 N (the load on femur's head) to the projection of the displacement of the middle of the femoral head into the load direction vector.

### 3.3. Comparison of numerical and experimental results

Inspecting ***all*** measurements (155 values), the FEA correlated with the EXP by 93% with a slope of the regression curve of 1.0093 (Fig. 7). The mean of the absolute deviations between FEA and EXP amounted to 22% for all measurements.

When looking at the strain measurements separately (60 values), the FEA correlated with the EXP by 95% with a slope of the regression curve of 1.0362 (Fig. 8). The mean of the absolute

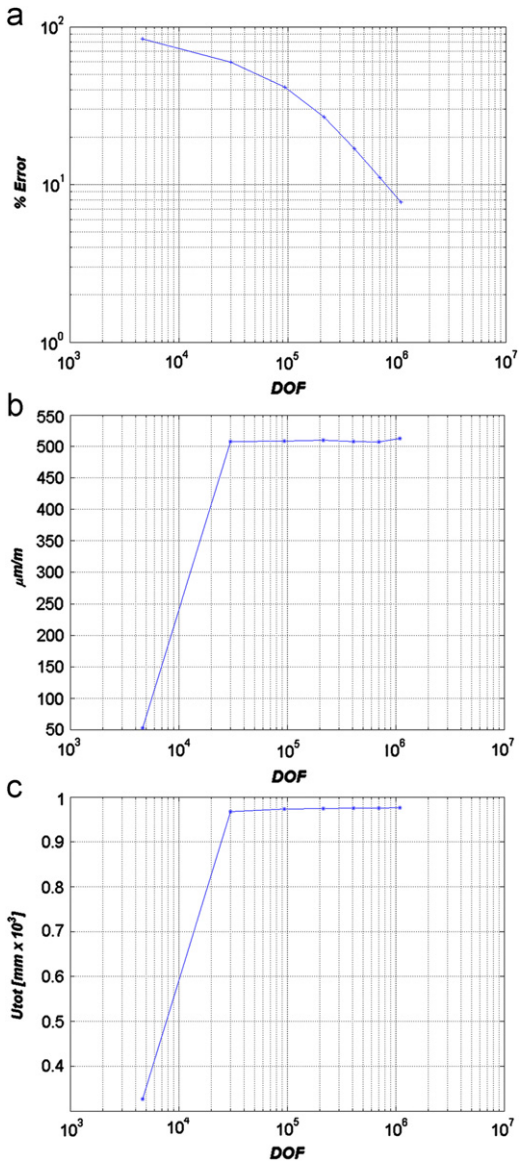


**Fig. 5.** Typical FE convergence for femur 1Left for $p=1$ to 8. (a) Convergence in energy norm. (b) Average strain convergence at SG4. (c) Point displacement convergence.

deviations between FEA and EXP amounted to 22% for the strain measurements.

Regarding the local total displacements on the bone surface (83 values), the FEA correlated with the EXP by 87% with a slope of the regression curve of 0.987 (Fig. 9). The mean of the absolute deviations between FEA and EXP amounted to 19% for the local displacements.

The mean of the experimental stiffness measurements amounted to $1311 \pm 330$ N/mm. For the stiffness measurements, the FEA correlated with the EXP by 62% with a slope of the regression curve of 1.3673 (Fig. 10). The mean of the absolute deviations between FEA and EXP amounted to 45% for the stiffness measurements.

## 4. Discussion

The aim of this study was to demonstrate the reliability of PSHOFE models. It has been shown that:

(a) qCT-based PSHOFE models are capable of predicting very well all *measured* quantities, i.e. displacement magnitudes and strains for a sufficiently sized sample of femurs taken from donors of both genders and a diversity of ages.

(b) The predictions are bias-free, as neither the group that performed the FEAs nor the group who performed the experiments knew of each other's results until both activities were completed.

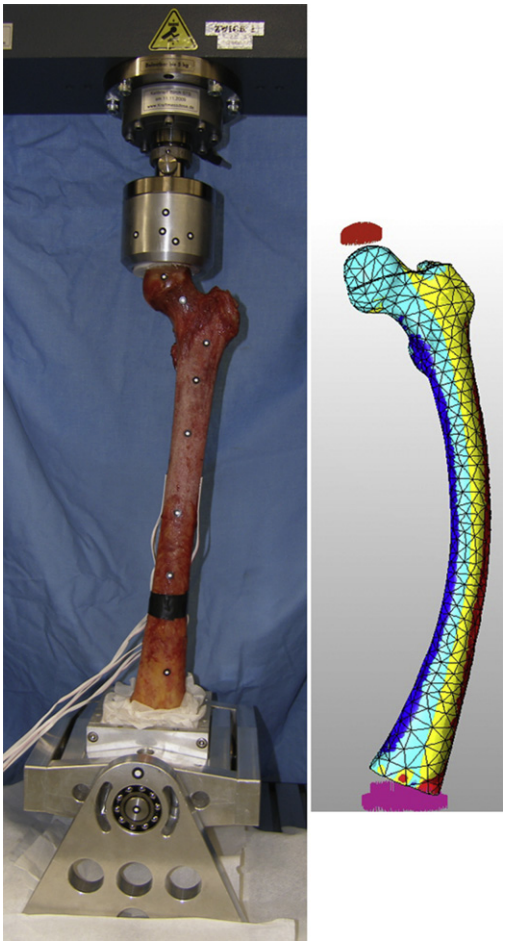

**Fig. 6.** Deformed FE femur (magnified) and its corresponding experiment.

We verified that the stiffness measurements are in good correlation with previous works. An excellent correlation is obtained between the mean stiffness in our experiments (1331 N/mm) with the value of 1360 N/mm reported in Cristofolini et al. (1996) obtained for 4 femurs loaded uniaxially at an inclination angle of 11°. In Papini et al. (2007) a larger cohort of 25 femurs was loaded uniaxially, but at an inclination angle of 15°, reporting an averaged stiffness of 757 N/mm with a standard deviation of 264 N/mm.

The good agreement between the analyses and experiments are to the best of the authors' knowledge more accurate as reported in the literature (as shown in Table 3) when strains are addressed, and moreover in the present study a very good agreement is noticed in the displacements also (not reported in other studies to the best of our knowledge).

The use of high-order FE methods with an accurate representation of bone's geometry, the continuous change of material properties within the femur and Young's modulus–density relation used in our PSHOFE analyses are believed to result in the very good prediction capabilities—see (Trabelsi et al., 2009). Having validated the PSHOFE results by a non-biased comparison, the methods are advocated for use and further development to pathological cases as osteoporosis and different fixation scenarios.

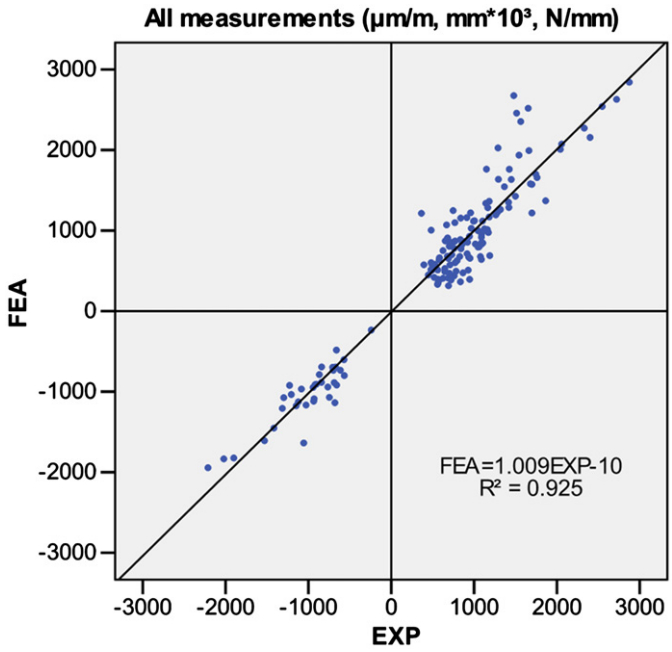


**Fig. 7.** All data (strains, displacements × 1000, stiffness): FEA vs. experimental results.

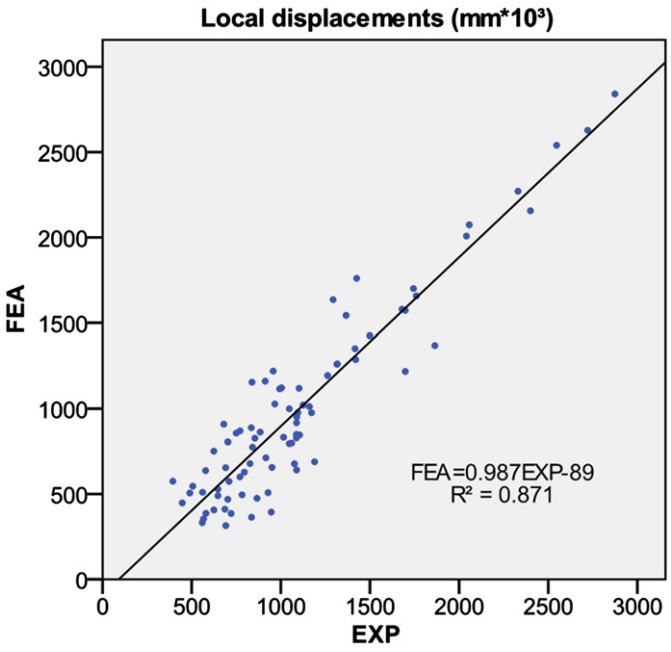


**Fig. 9.** FEA displacements × 1000 vs. experimental results.

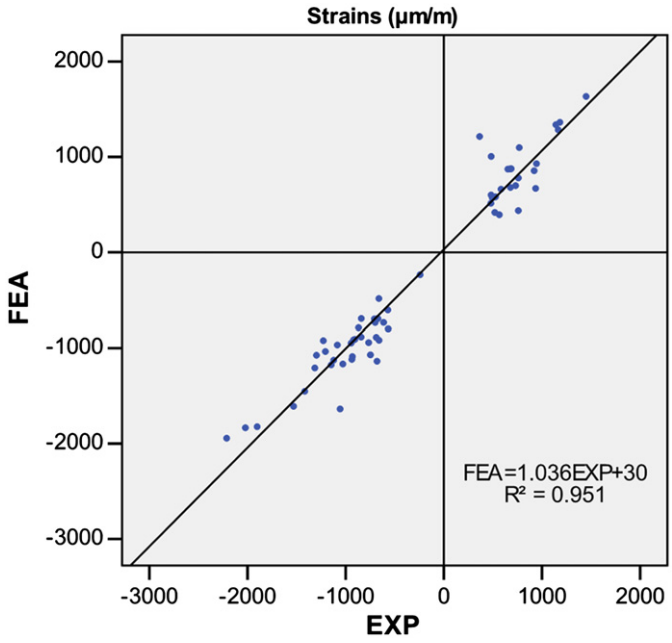


**Fig. 8.** FEA strains vs. experimental results.

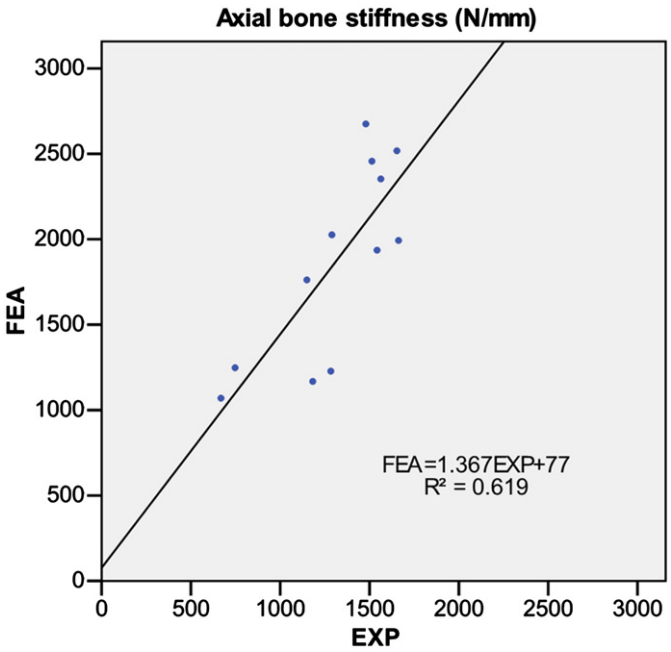


**Fig. 10.** FEA bone stiffness vs. experimental results.

Limitations of the present work are: (a) The FE model did not take into account the known local anisotropic behavior of the bone tissue. (b) Only five uniaxial strain gauges were bonded to each bone, in the anticipated principal directions. (c) The overall stiffness of the bone was computed by using an approximated value of the adapter displacement. (d) A simplified stance position loading was considered. The validation would have been more complete if multiple and more complex loading conditions could have been applied in the experiments (we considered herein a "stance position" loading where axial load and bending moment were excited in the bone). For this loading condition, we have demonstrated that an isotropic inhomogeneous material with the empirical connection given in Keyak and Falkinstein (2003) in conjunction with a high-order finite element model results in predictions which very well represent the in-vitro experimental observations. These limitations are currently considered and investigated, to be reported in a future publication.

The overall bone stiffness of the PSHOFE models was shown to be higher compared to the "measured stiffness" by about 35%. This discrepancy is attributed to the different interpretation of "stiffness" between the experiment and the computation, and the simplified boundary conditions in the FEA. Whereas in the experiment the displacement of the loading device was used to compute the stiffness, in the FE models because the rigid cup was not modeled and neither was the contact between the head and the adapter considered, we computed the stiffness by using the

**Table 3**
Match between FE analyses and experimental results in previous recent publications compared to present results.

| Ref | # of femurs (# of data points) | $R^2$ | Slope | Remarks |
|---|---|---|---|---|
| Helgason et al. (2008b) | 1 femur (13 rosettes–5 different loadings) | 0.85 | 1.5 | Principle strains |
| Schileo et al. (2007) | 8 femurs (120 SGs) | 0.91 | 1.01 | Principle strains |
| Schileo et al. (2008) | 8 femurs (120 SGs) | 0.95 | 0.97 | Principle strains (same experiments E(rho) relations) |
| Bessho et al. (2007) | 11 femurs (12 rosettes per femur. Not clear which strain measures used.) | 0.927 | 0.91 | Strains—the strain measure N/A, and neither the clear the number of data points and no graphs are presented |
| Present, strains only | 12 femurs (60 SGs) | 0.95 | 1.036 | SGs along assumed principle strains |
| Present, displacements and strains | 12 femurs (155 data points) | 0.93 | 1.009 | |

displacement at the middle of the head (which of course is a bit different). Future studies are intended to more accurately represent the rigid cup and its contact with the load adapter, to demonstrate that the stiffness prediction is merely a local modeling imprecision. This however, does not have an effect on the validity of the strain and displacements computations.

To conclude, a method for constructing patient-specific p-FE models from qCT scans was used in this study on a sample size not yet considered in the past, and more importantly compared to experiments in a douple-blinded manner. An excellent agreement has been demonstrated between the analyses and experiments both in displacements and strains (although the over-stiff response). The discrepancies between the predictions and experiments reported in this study are considered excellent for a biomechanical analysis in light of the sample size and blinding. This study exemplifies that the presented method is in an advanced stage to be used in clinical computer-aided decision making.

## Conflict of interest statement

None declared.

## Acknowledgments

The first two authors acknowledge the generous support of the Technical University of Munich—Institute for Advanced Study, funded by the German Excellence Initiative.

## Appendix A. Supplementary material

Supplementary data associated with this article can be found in the online version at doi:10.1016/j.jbiomech.2011.03.024.

## References

Bessho, M., Ohnishi, I., Matsuyama, J., Matsumoto, T., Imai, K., Nakamura, K., 2007. Prediction of strength and strain of the proximal femur by a CT-based finite element method. J. Biomechanics 40, 1745–1753.

Cody, D.D., Hou, F.J., Divine, G.W., Fyhrie, D.P., 2000. Short term in vivo study of proximal femoral finite element modeling. Ann. Biomed. Eng. 28, 408–414.

Cody, D.D., Gross, G.J., Hou, F.J., Spencer, H.J., Goldstein, S.A., Fyhrie, D.P., 1999. Femoral strength is better predicted by finite element models than QCT and DXA. J. Biomech. 32, 1013–1020.

Cristofolini, L., Viceconti, M., Cappello, A., Toni, A., 1996. Mechanical validation of whole bone composite femur models. J. Biomech. 29 (4), 525–535.

Eberle, S., Gerber, C., von Oldenburg, G., Hungerer, S., Augat, P., 2009. Type of hip fracture determines load share in intramedullary osteosynthesis. Clin. Orthop. Relat. Res. 467, 1972–1980.

Helgason, B., Perilli, E., Schileo, E., Taddei, F., Brynjolfsson, S., Viceconti, M., 2008a. Mathematical relationships between bone density and mechanical properties: a literature review. Clin. Biomech. 23, 135–146.

Helgason, B., Taddei, F., Palsson, H., Schileo, E., Cristofolini, L., Brynjolfsson, M., Vicecont, S., 2008b. A modified method for assigning material properties to FE models of bones. Med. Eng. Phys. 30, 444–453.

Keaveny, T.M., 2010. Biomechanical computed tomography—noninvasive bone strength analysis using clinical computed tomography scans. Ann. N. Y. Acad. Sci. 1192, 65–75.

Keller, T.S., 1994. Predicting the compressive mechanical behavior of bone. J. Biomech. 27, 1159–1168.

Keyak, J., Falkinstein, Y., 2003. Comparison of in situ and in vitro CT scan-based finite element model predictions of proximal femoral fracture load. Med. Eng. Phys. 25, 781–787.

Keyak, J.H., Meagher, J.M., Skinner, H.B., Mote Jr., C.D., 1990. Automated three dimensional finite element modelling of bone: a new method. J. Biomed. Eng. 12, 389–397.

Morgan, E.F., Bayraktar, H.H., Keaveny, T.M., 2003. Trabecular bone modulus–density relationships depend on anatomic site. J. Biomechanics 36, 897–904.

Papini, M., Zdero, R., Schemitsch, E.H., Zalzal, P., 2007. The biomechanics of human femurs in axial and torsional loading: comparison of finite element analysis, human cadaveric femurs, and synthetic femurs. J. Biomech. Eng.—Trans. ASME 129, 12–19.

Schileo, E., Dall'Ara, E., Taddei, F., Malandrino, A, Schotkamp, T., Viceconti, M., Baleani, M., 2008. An accurate estimation of bone density improves the accuracy of subject-specific finite element models. J. Biomech. 41 (11), 2483–2491.

Schileo, E., Taddei, F., Malandrino, A., Cristofolini, L., Viceconti, M., 2007. Subject-specific finite element models can accurately predict strain levels in long bones. J. Biomech. 40, 2982–2989.

Speirs, A.D., Heller, M.O., Duda, G.N., Taylor, W.R., 2007. Physiologically based boundary conditions in finite element modelling. J. Biomech. 40, 2318–2323.

Szabo, B., Babuska, I., 1991. Finite Element Analysis. Wiley.

Taddei, F., Schileo, E., Helgason, B., Cristofolini, L., Viceconti, M., 2007. The material mapping strategy influences the accuracy of CT-based finite element models of bones: an evaluation against experimental measurements. Med. Eng. Phys. 29, 973–979.

Taddei, F., Cristofolini, L., Martelli, S., Gill, H.S., Viceconti, M., 2006. Subject-specific finite element models of long bones: an in vitro evaluation of the overall accuracy. J. Biomech. 39, 2457–2467.

Trabelsi, N., Yosibash, Z., Milgrom, C., 2009. Validation of subject specific automated p-FE analysis of the proximal femur. J. Biomech. 42, 234–241.

Yosibash, Z., Trabelsi, N., Milgrom, C., 2007a. Reliable simulations of the human proximal femur by high-order finite element analysis validated by experimental observations. J. Biomech. 40, 3688–3699.

Yosibash, Z., Padan, R., Joscowicz, L., Milgrom, C., 2007b. A CT-based high-order finite element analysis of the human proximal femur compared to in-vitro experiments. ASME J. Biomech. Eng. 129 (3), 297–309.